

Forecast sensitivity to observation (FSO) as a diagnostic tool

Carla Cardinali

Research Department

Document presented to the 38th Session of the
Scientific Advisory Committee

October 2009

This paper has not been published and should be regarded as an Internal Report from ECMWF.
Permission to quote from it should be obtained from the ECMWF.



European Centre for Medium-Range Weather Forecasts
Europäisches Zentrum für mittelfristige Wettervorhersage
Centre européen pour les prévisions météorologiques à moyen

Series: ECMWF Technical Memoranda

A full list of ECMWF Publications can be found on our web site under:

<http://www.ecmwf.int/publications/>

Contact: library@ecmwf.int

© Copyright 2009

European Centre for Medium Range Weather Forecasts
Shinfield Park, Reading, Berkshire RG2 9AX, England

Literary and scientific copyrights belong to ECMWF and are reserved in all countries. This publication is not to be reprinted or translated in whole or in part without the written permission of the Director. Appropriate non-commercial use will normally be granted under the condition that reference is made to ECMWF.

The information within this publication is given in good faith and considered to be true, but ECMWF accepts no liability for error, omission and for loss or damage arising from its use.

Abstract

This paper describes the use of forecast sensitivity to observations as a diagnostic tool to monitor the observation impact on the quality of the short range forecasts (typically 24 hour). The forecast error is provided by a control experiment (using all observations available) which has been run among two series of observing system experiments performed at ECMWF. The observation data impact obtained with the forecast sensitivity is then compared with the observation data impact as classically measured in the context of observing system experiments. Differences and similarities between the two approaches are highlighted. Overall, the assimilated observations decrease the forecast error. However, locally some poor performances are detected that are related either to the data quality, the sub-optimality of the data assimilation system or biases in the model. It is also found that some synoptic situation can deteriorate the quality of certain measurements or can induce some local weather variability over small areas that the assimilation system cannot correctly resolve. Finally, the performance of the current operational version (CY35R2) of the data assimilation system for the last four months of 2008 shows a consistent overall positive impact of the observations.

1 Introduction

Over the last decade, data assimilation schemes have evolved towards very sophisticated systems, such as the four-dimensional variational system (4D-Var) (Rabier *et al.* 2000) that operates at the European Centre for Medium-Range Weather Forecasts (ECMWF). The scheme handles a large variety of both space and surface-based meteorological observations. It combines the observations with prior (or background) information on the atmospheric state and uses a comprehensive (linearized) forecast model to ensure that the observations are given a dynamically realistic, as well as statistically likely response in the analysis. Effective performance monitoring of such a complex system, with an order of 10^7 degrees of freedom and more than 10^6 observations per 12-hour assimilation cycle, has become an absolute necessity.

The assessment of each observation contribution to the analysis is among the most challenging diagnostics in data assimilation and numerical weather prediction. Methods have been derived to measure the observational influence in data assimilation schemes (Purser and Hung 1993, Cardinali *et al.* 2004, Fisher 2003, and Chapnick *et al.* 2004). These techniques show how the influence is assigned during the assimilation procedure, which partition is given to the observation and which is given to the background or pseudo-observation. They therefore provide a indication of the robustness of the fit between model and observations and allow some tuning of the weights assigned in the assimilation system.

Recently, adjoint-based observation sensitivity techniques have been used (Baker and Daley 2000, Langland and Baker 2004, Cardinali and Buizza, 2004, Morneau *et al.*, 2006, Xu and Langlang, 2006, Zhu and Gelaro 2008) to measure the observation contribution to the forecast, where the observation impact is evaluated with respect to a scalar function representing the short-range forecast error. In general, the adjoint methodology can be used to estimate the sensitivity measure with respect to any parameter of importance of the assimilation system. Very recently, Daescu (2008) derived a sensitivity equation of an unconstrained variational data assimilation system from the first order necessary condition with respect to the main input parameters: observation, background and their error covariance matrices. The paper provides the theoretical framework for further diagnostic tool development not only to evaluate the observation impact on the forecast but also the impact of the other analysis parameters. Sensitivity to background covariance matrix can help in evaluating the correct specification of the background weight and their correlation. Limitations and weaknesses of the covariance matrices are well known, several assumptions and simplifications are

made to derive them. Desroziers and Ivanov (2001) and Chapnik et al. (2006) discussed the importance of diagnosing and tuning the error variances in a data assimilation scheme.

Over the past years, Observing System Experiments (OSEs) have been the traditional tool for estimating data impact in a forecasting system (Bouttier and Kelly, 2001 English *et al.*, 2004 and Lord *et al.*, 2004, Kelly and Thépaut, 2007). Usually, OSEs are performed by removing subsets of observation from the assimilation system and the forecasts are compared against a *control* experiment that includes all observations.

The value of observations in the forecast is assessed by comparing forecast skill obtained by different statistical measures and several independent experiments need to be performed for quite long periods (a few months) to ensure statistical significance to the results. The assessment of the value of a given observation type can become quite expensive if a full investigation of the different components of the GOS (Global Observing System) is performed.

Clearly, there are some basic differences between the adjoint-based observation technique and the OSE technique:

- The adjoint-based observation sensitivity technique measures the impact of observations when the entire observation dataset is present in the assimilation system, while the observing system is, in the OSE context, modified. In fact, each OSE experiment differs from the others in terms of assimilated observations.
- The adjoint-based observation sensitivity technique measures the response of a single forecast metric to all perturbations of the observing system, while the OSE measures the effect of a single perturbation on all forecast metrics.
- The adjoint-based technique is restricted by the tangent linear assumption, valid up to 3 days. Furthermore, a simplified adjoint model is usually used to carry the forecast error information backwards, which limits further the validity of the linear assumption, and therefore restricts the use of the diagnostic to a typical forecast range of 24-48 hours. One implication to use a simplified adjoint model is that the analysis uncertainties obtained throughout the adjoint integration can be incorrect if the propagating back signal is weak (Isakseen et al., 2005). The OSE on the other hand can measure data impact on long-range forecast.
- The adjoint-based observation sensitivity technique measures the impact of all observations assimilated at a single analysis time while the OSE includes effect of observations assimilated at previous time since they compare modified Kalman gain matrices.

The aim of this paper is twofold: illustrate the type of investigation and diagnostics that can be carried out with the adjoint-based observation sensitivity in an operational context, and provide the overall observation performance in the system. To this respect the adjoint tool is based on the forecast error of the *control* experiment of those OSEs that have recently been performed at ECMWF (Kelly and Thépaut 2007) and on the forecast error of the last implemented operational model.

In this paper, the potential of estimating forecast sensitivity to observations as a diagnostic tool to investigate the sources of short-range forecast errors is shown and qualitatively contrasted with an Observing System

Experiment data impact tool. In section 2, the theoretical background of the forecast sensitivity (observation and background), the numerical solution and the calculation of the forecast error contribution from observations are shown. Also, the OSEs used in the investigation are summarized. Results are illustrated in section 3. Section 4 shows the performance of the ECMWF operational configuration with respect to the current observation network. Conclusions are given in section 5.

2 Observation impact on the forecast

2.1 Linear analysis equation

Data assimilation systems for numerical weather prediction (NWP) provide estimates of the atmospheric state \mathbf{x} by combining meteorological observations \mathbf{y} with prior (or background) information \mathbf{x}_b . A simple Bayesian normal model provides the solution as the posterior expectation for \mathbf{x} , given \mathbf{y} and \mathbf{x}_b . The same solution can be achieved from a classical *frequentist* approach, based on a statistical linear analysis scheme providing the Best Linear Unbiased Estimate (Talagrand 1997) of \mathbf{x} , given \mathbf{y} and \mathbf{x}_b . The optimal general least square solution to the analysis problem (see Lorenc 1986) can be written

$$\mathbf{x}_a = \mathbf{K}\mathbf{y} + (\mathbf{I}_n - \mathbf{K}\mathbf{H})\mathbf{x}_b \quad 2.1$$

The vector \mathbf{x}_a is called the ‘analysis’. The gain matrix \mathbf{K} (of dimension $n \times p$ with n being the state vector and p the observation vector dimensions) takes into account the respective accuracies of the background vector \mathbf{x}_b and the observation vector \mathbf{y} as defined by the $(n \times n)$ -dimensioned covariance matrix \mathbf{B} and the $(p \times p)$ -dimensioned covariance matrix \mathbf{R} , with

$$\mathbf{K} = (\mathbf{B}^{-1} + \mathbf{H}^T \mathbf{R}^{-1} \mathbf{H})^{-1} \mathbf{H}^T \mathbf{R}^{-1} \quad 2.2$$

Here, \mathbf{H} is a $(p \times n)$ -dimensioned matrix interpolating the background fields to the observation locations, and transforming the model variables to observed quantities (e.g. radiative transfer calculations transforming the model’s temperature, humidity and ozone into brightness temperatures as observed by several satellite instruments). In the 4D-Var context, \mathbf{H} also includes the propagation in time of the atmospheric state vector to the observation times using a forecast model. From (2.1) the sensitivity of the analysis system with respect to the observations and the background can be derived from:

$$\begin{aligned} \frac{\partial \mathbf{x}_a}{\partial \mathbf{y}} &= \mathbf{K}^T \\ \frac{\partial \mathbf{x}_a}{\partial \mathbf{x}_b} &= \mathbf{I} - \mathbf{H}^T \mathbf{K}^T \end{aligned} \quad 2.3$$

The analysis sensitivity with respect to the observation is a similar measure as the observation influence derived by Cardinali *et al.* (2004). The only difference to the ‘influence matrix’ is the space in which the solution is found. Here, the analysis sensitivity is found in the model space instead of the observation space.

2.2 Sensitivity gradient

Let consider two forecasts of length f starting from \mathbf{x}_a and length g starting from \mathbf{x}_b , \mathbf{x}_b being the background field used in the \mathbf{x}_a analysis. Both forecasts verify at time t . Following Langland and Baker (2004) and Errico (2007) the third order sensitivity gradient is defined as

$$\frac{\partial J}{\partial \mathbf{x}_a} = \frac{\partial J_f}{\partial \mathbf{x}_a} + \frac{\partial J_g}{\partial \mathbf{x}_a} \quad 2.4$$

Where $J_f = \langle (\mathbf{x}_f - \mathbf{x}_t), \mathbf{C}(\mathbf{x}_f - \mathbf{x}_t) \rangle / 2$ and $J_g = \langle (\mathbf{x}_g - \mathbf{x}_t), \mathbf{C}(\mathbf{x}_g - \mathbf{x}_t) \rangle / 2$ are a quadratic measure of the two forecast errors (\mathbf{x}_t the verifying analysis, taken here as the truth), and \mathbf{C} is a matrix of dry energy norm weighting coefficients. It is clear that from (2.4) the adjoint model maps the sensitivity (with respect to the forecast) of J_f into $\partial J_f / \partial \mathbf{x}_a$ along the trajectory f and the sensitivity of J_g into $\partial J_g / \partial \mathbf{x}_a$ along the trajectory g (see Rabier *et al.* 1996, Gelaro *et al.*, 1998 for the first order sensitivity gradient definition and computation).

2.3 Sensitivity equation

Baker and Daley (2000) derived the forecast sensitivity equation with respect to the observations in the context of variational data assimilation. Let us consider a scalar J -function of the forecast error. Then, the sensitivity of J with respect to the observations can be written using a simple derivative chain as:

$$\frac{\partial J}{\partial \mathbf{y}} = \frac{\partial J}{\partial \mathbf{x}_a} \frac{\partial \mathbf{x}_a}{\partial \mathbf{y}} \quad 2.5$$

where $\partial J / \partial \mathbf{x}_a$ is the sensitivity of the forecast error to the initial condition described in section 2.2. By using eq.(2.2) and (2.3) the forecast sensitivity to the observations becomes:

$$\frac{\partial J}{\partial \mathbf{y}} = \mathbf{K}^T \frac{\partial J}{\partial \mathbf{x}_a} = \mathbf{R}^{-1} \mathbf{H} (\mathbf{B}^{-1} + \mathbf{H}^T \mathbf{R}^{-1} \mathbf{H})^{-1} \frac{\partial J}{\partial \mathbf{x}_a} \quad 2.6$$

where $(\mathbf{B}^{-1} + \mathbf{H}^T \mathbf{R}^{-1} \mathbf{H})^{-1}$ is the analysis error covariance matrix \mathbf{A} .

2.4 Numerical solution

In an optimal variational analysis scheme, the analysis error covariance matrix \mathbf{A} is approximately the inverse of the matrix of second derivatives (the Hessian) of the analysis cost function J_a (Rabier *et al.* 2000), i.e. $\mathbf{A} = (\mathbf{J}_a'')^{-1}$ (Rabier and Courtier 1992). Given the large dimension of the matrices involved, \mathbf{J}_a'' and its inverse cannot be computed explicitly. The minimization is performed in terms of a transformed variable $\boldsymbol{\chi}$, $\boldsymbol{\chi} = \mathbf{L}^{-1}(\mathbf{x} - \mathbf{x}_b)$, with \mathbf{L} chosen such that $\mathbf{B} = \mathbf{L}\mathbf{L}^T$. The transformation \mathbf{L} thus reduces the covariance of the prior to the identity matrix. In variational data assimilation, \mathbf{L} is referred to as the change-of-variable operator (Courtier *et al.* 1998). Now apply the change-of-variable in the analysis cost function and write:

$$\begin{aligned} J_a(\mathbf{x}) &= \frac{1}{2} (\mathbf{x} - \mathbf{x}_b)^T \mathbf{B}^{-1} (\mathbf{x} - \mathbf{x}_b) + \frac{1}{2} (\mathbf{H}\mathbf{x} - \mathbf{y})^T \mathbf{R}^{-1} (\mathbf{H}\mathbf{x} - \mathbf{y}) \\ &= \frac{1}{2} \boldsymbol{\chi}^T \boldsymbol{\chi} + \frac{1}{2} (\mathbf{H}\mathbf{L}\boldsymbol{\chi} - \mathbf{y})^T \mathbf{R}^{-1} (\mathbf{H}\mathbf{L}\boldsymbol{\chi} - \mathbf{y}) = J_a(\boldsymbol{\chi}) \end{aligned} \quad 2.7$$

The Hessian becomes:

$$J_a''(\boldsymbol{\chi}) = \mathbf{I} + \mathbf{L}^T \mathbf{H}^T \mathbf{R}^{-1} \mathbf{H} \mathbf{L} \quad 2.8$$

By applying the change-of-variable in (2.7) and by using (2.8), the forecast sensitivity to the observations is expressed as:

$$\frac{\partial J}{\partial \mathbf{y}} = \mathbf{R}^{-1} \mathbf{H} \mathbf{L} (\mathbf{I} + \mathbf{L}^T \mathbf{H}^T \mathbf{R}^{-1} \mathbf{H} \mathbf{L})^{-1} \mathbf{L}^T \frac{\partial J}{\partial \mathbf{x}_a} \quad 2.9$$

Using the conjugate gradient algorithm, first the following equation for $\partial J / \partial \mathbf{y} = \mathbf{R}^{-1} \mathbf{H} \mathbf{z}$ is solved:

$$\begin{aligned} (\mathbf{I} + \mathbf{L}^T \mathbf{H}^T \mathbf{R}^{-1} \mathbf{H} \mathbf{L}) \mathbf{z} &= \mathbf{L} \mathbf{z}_a \\ \mathbf{z}_a &= \frac{\partial J}{\partial \mathbf{x}_a} \end{aligned} \quad 2.10$$

The solution \mathbf{z} lies in the Krylov-subspace generated by the vector $\mathbf{L}^T \mathbf{z}_a$ and the matrix $(\mathbf{I} + \mathbf{L}^T \mathbf{H}^T \mathbf{R}^{-1} \mathbf{H} \mathbf{L})$. The Krylov-subspace dimension is the degree of the minimal polynomial of $(\mathbf{I} + \mathbf{L}^T \mathbf{H}^T \mathbf{R}^{-1} \mathbf{H} \mathbf{L})$. Therefore if the degree is low, the Krylov-method searches the solution on a small dimensioned space. The method is very efficient in an iterative solution of a linear system with large and sparse matrices (Van der Vorst 2003).

The forecast sensitivity to observations is then given by interpolating \mathbf{z} (using the \mathbf{H} operator) in the observation space and by normalizing with respect to the observation error covariance matrix \mathbf{R} .

2.5 Observation impact measure

Once the forecast sensitivity is computed, the variation δJ of the forecast error expressed by J can be found by rearranging (2.1) and by using the adjoint property for the linear operator:

$$\delta J = \left\langle \frac{\partial J}{\partial \mathbf{x}_a}, \delta \mathbf{x}_a \right\rangle = \left\langle \frac{\partial J}{\partial \mathbf{x}_a}, \mathbf{K}(\mathbf{y} - \mathbf{H} \mathbf{x}_b) \right\rangle = \left\langle \mathbf{K}^T \frac{\partial J}{\partial \mathbf{x}_a}, \mathbf{y} - \mathbf{H} \mathbf{x}_b \right\rangle = \left\langle \mathbf{K}^T \frac{\partial J}{\partial \mathbf{x}_a}, \delta \mathbf{y} \right\rangle = \left\langle \frac{\partial J}{\partial \mathbf{y}}, \delta \mathbf{y} \right\rangle \quad 2.11$$

where $\delta \mathbf{x}_a = \mathbf{x}_a - \mathbf{x}_b$ are the analysis increments and $\delta \mathbf{y} = \mathbf{y} - \mathbf{H} \mathbf{x}_b$ is the innovation vector. This is the first time that δJ has been computed for a 12 hour 4D-Var system; the sensitivity gradient $\partial J / \partial \mathbf{x}_a$ is valid at the starting time of the 4D-Var window (typically 09 and 21 UTC for the 12h 4D-Var set-up used at ECMWF). As for \mathbf{K} , its adjoint \mathbf{K}^T incorporates the temporal dimension, and the $\delta \mathbf{y}$ innovations are distributed over the 12-hour window. The variation of the forecast error due to a specific measurement can be summed up over time and space in different subsets to compute the average contribution of different component of the observing system to the forecast error. For example, the contribution of all AMSU-A satellite instruments, s , and channels, i , over time T will be:

$$\delta J_{AMSU-A} = \sum_{s \in S} \sum_{\substack{i \in \text{channel} \\ t \in T}} \delta J_{it}^s$$

The forecast error contribution can be gathered over different subsets that can represent a specific observation type, a specific vertical or horizontal domain, or a particular meteorological variable.

2.6 Observation System Experiment

A traditional way of estimating data impact in a forecasting system is to perform OSEs such as those illustrated by Bouttier and Kelly (2001) or Kelly and Thépaut (2007) (for other weather centres see also

English *et al.* 2004 and Lord *et al.* 2004). OSEs can be performed in two ways: in one way, the performance of a baseline (*reference*) experiment which uses a minimum amount of observation types is compared with experiments that add at least one more observation type (Kelly and Thépaut, 2007). The other way consists in removing one particular or various datasets from the full system over a long assimilation period and to then compare the performance with respect to the *control* experiment, which assimilates the fully available observations from the GOS. In either case, it has to be reminded that removing observations from the assimilation system will generate a different Kalman gain matrix.

Table 1: Operational data set in the OSE control experiment for summer 2006 and winter 2007 (Kelly and Thépaut, 2007). *T, H, RH, p, u* and *v* stand for temperature, humidity, relative humidity, pressure and *u* and *v* wind components.

Type of Data	Description
OZONE	Satellite ozone retrieval
GOES	Geostationary satellite infrared sounder radiances
METEOSAT	Geostationary satellite infrared sounder radiances
AMSU-B	Satellite microwave sounder radiances related to H
SSMI-TCWV	Satellite microwave imager radiances related to clouds and precipitation
SSMI	Satellite microwave imager radiances related to H and surface wind speed
AIRS	Satellite infrared sounder radiances related to H and T
AMSU-A	Satellite microwave sounder radiances related to T
HIRS	Satellite infrared radiances
ERS-QuikSCAT	Satellite microwave scatterometer
AMVs	Atmospheric Motion Vectors derived from satellite cloud imagery
GPS-RO	Satellite GPS radio occultation
PILOT	Sondes and American, European and Japanese Wind profiler (u,v)
TEMP	Radiosondes from land and ship measuring ps, T, RH, u and v
AIREP	Aircraft measurements of T, u and v
DRIBU	Drifting buoy measuring ps, T, RH, u and v
SYNOP	Surface Observations from land and ship stations: measuring ps, RH, u and v

Table 2: List of OSEs.

Name	Observations assimilated
Reference	Conventional, AMSU-A from NOAA-16.
AMV	Reference + AMVs
SCAT	Reference + ERS scatterometer+ QuikSCAT
Control	All data without GPS-RO
GPSRO	All data with GPS-RO

The assessment of the observation value with respect the forecast skill through OSEs is performed by e.g. comparing the root mean square forecast error, anomaly correlation, etc. obtained with and without the subset of interest. This usually involves several independent experiments over a few months. Therefore, OSEs can be quite costly if a comprehensive investigation of the various contributions of the elements of the GOS needs to be performed. In Table 1 and Table 2, the observations assimilated in the *control* experiment and the list of the OSEs used in the investigation, are summarized. Forecasts have been computed for each OSEs from the 00 UTC analyses only, in order to save computing time.

3 Results

The forecast sensitivity to the observation (FSO) has been computed for two seasons, a winter and a summer period, based on the forecast error calculated for the *control* experiment of the OSEs performed by Kelly and Thépaut (2007). The FSO calculation [(2.9) and (2.10)] has been carried out on 60 model levels and with a horizontal truncation of T159 to match with the OSE final inner loop resolution and also based on both 00 and 12 UTC forecast error (only the 00 impact is shown). As for the OSE, the observation departures were computed at T511 (model trajectory resolution, Rabier *et al.* 2000). All the experiments were performed using the third order sensitivity gradient defined in section 2(b). A comparison of the FSO using the first order sensitivity gradient, based on a global square dry energy norm diagnostic function $J_1 = \|\mathbf{e}_t, \mathbf{C}\mathbf{e}_t\|$ (Rabier *et al.* 1996) with \mathbf{e} computed at $t=24$, is also shown in the following section 3(b). Sensitivity gradients were computed at T159 analysis resolution.

The sensitivity to the humidity initial condition is obtained as a secondary effect due to the adjoint of the linearized moist physical processes used in the sensitivity gradient calculation (Lopez and Moreau 2005, Tompkins and Janisková 2004, Janisková *et al.* 2002) which accounts for the dependency of the forecast error at the verification time due to the humidity errors in the initial conditions. The energy norm diagnostic function was computed from the OSE *control* (using all available observations) experiment forecast error.

In the results presented here, the potential of the FSO diagnostic tool on the contribution of the observing system to the short-range forecast error is investigated and contrasted with that from the OSE tool. Due to the fact that the OSEs medium-range forecast is computed only from the 00 UTC analyses, the FSO diagnostic, when compared to the OSE diagnostic, is also shown for the 00 UTC analysis cycles.

3.1 Third order sensitivity gradient

3.1.1 Summer

The impact of the operational data set on the 24 hour forecast error has been investigated for the period 15 June to 15 July 2006 at 00 and 12 UTC (summer 2006). The forecast error for which the FSO is based is computed from the *control* experiment of the OSEs (see Table 1 and Table 2). The global observation performance over this period, as described in eq.(2.11), is summarized in Figure 1. Negative (positive) values correspond to a decrease (increase) of forecast error due to a specific observation type. The range of the results accuracy is estimated to be ~16%, therefore small negative and small positive values should be regarded quantitatively as neutral observation impact. Nonetheless, degradation observed in the error range can bring useful information on the possible causes affecting the data performance on the forecast, as will be shown.

In future, a statistical estimation of the relative observation type error, will be computed and displayed, in fact, a number of sufficient FSO integrations needed for a significant estimate.

The largest error decrease is due to AMSU-A (four satellites) and AIRS radiances followed by SYNOP (mainly surface pressure), AIREP and DRIBU (mainly surface pressure) conventional observations. Good error reduction is also observed from SCAT (Quikscat and ERS scatterometer) and AMSU-B radiance

observations. An increase of forecast error is caused by AMVs (Atmospheric Motion Vector) from geostationary satellites. Some degradation is also observed from PILOT observations.

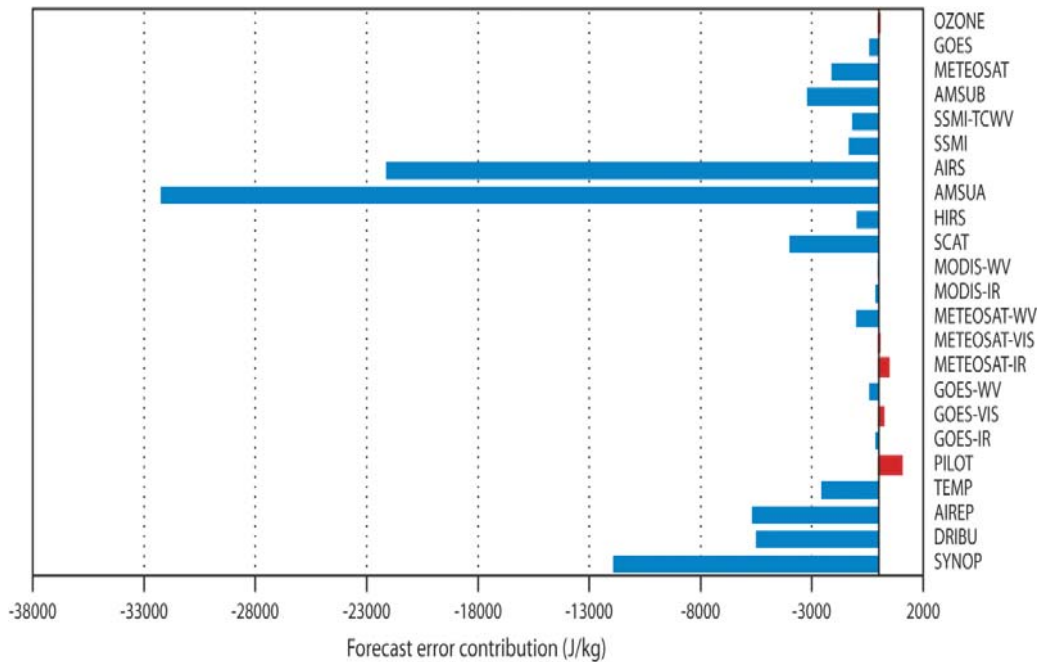


Figure 1: 24-hour forecast error contribution (third order sensitivity gradient) in J/kg of the components (types) of the observing system in summer 2006. Negative (positive) values correspond to a decrease (increase) in the energy norm of forecast error.

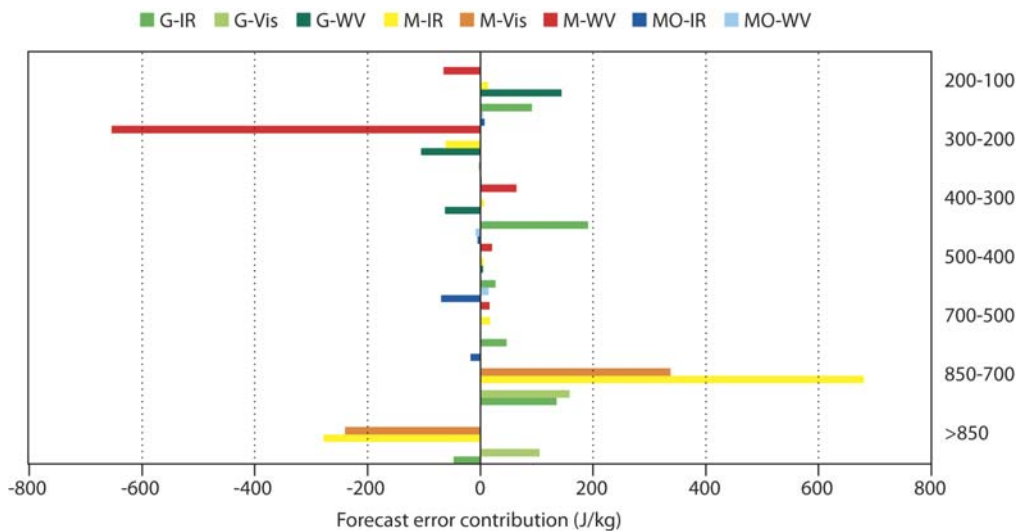


Figure 2: Forecast error contribution (third order sensitivity gradient) of the observed u-component of the wind on pressure levels and grouped by satellite types: GOES (G, two satellites GOES-8 and 9), METEOSAT (M, two satellite METEOSAT-7 and 8) and MODIS (MO, two satellites: Terra and Aqua) and by frequency bands: infrared (IR), visible (V) and water vapour (WV). Negative (positive) values correspond to a decrease (increase) of forecast error.

A more detailed diagnostic of the forecast error contribution from AMVs is shown in Figure 2. The contribution to the forecast error of the observed u-wind component is grouped by pressure levels, satellite types, such as GOES (G, two geostationary satellites GOES-8 and 9), METEOSAT (M, two geostationary

satellites METEOSAT-7 and 8) and MODIS polar instruments (MO, MODIS Terra and Aqua), and by frequency bands: infrared (IR), visible (V) and water vapour (WV). The largest degradation is due to the visible and infrared frequency band at levels below 700 hPa, (mainly at 850 hPa) from METEOSAT (to a larger extent) and from the GOES satellites.

The geographical locations of the degradation are shown in Figure 3 which displays the 00 UTC forecast error contribution of the visible and infrared bands between 1000 and 700 hPa accumulated over the summer month. The largest degradation is found over the southern equatorial band, in particular over the Atlantic (area-1) and Indian Ocean (area-2) where the METEOSAT satellites are located, followed by the one over the West Pacific (area-3) where GOES is operated. In the Indian Ocean, a well established Indian Monsoon circulation was taking place, characterized by a strong low level wind from South-East towards the Indian continent. Such a situation is not well represented by the model that tends to reinforce too much the low level circulation. The degradation due to the AMV in the area-2 is therefore likely attributed to a model bias. On the contrary, over the South of the Atlantic ocean (area-1) due to the presence of semi-permanent anti-cyclone circulation in the tropical band, the associated large scale subsidence reinforces the trade inversion with a subsequent suppression of deep clouds (around 30 degrees), leaving only the shallow ones. This synoptic situation has implication with the methodology applied by the data provider to measure the height of the top of the clouds, resulting in a degradation of the data quality. A modified analysis experiment by reassigning the height of the top of the clouds according to the model first guess instead of using the height assigned by the data provider (courtesy of Niels Bormann) was performed to address the point. Unfortunately, the FSO based on the new forecast error does not indicate a significant improvement. The causes of the degradations are still under investigation. Similar synoptic situation to area-2 is also noticed in area-3, it is therefore believed that, even for this case, the degradation is attributed to the data quality.

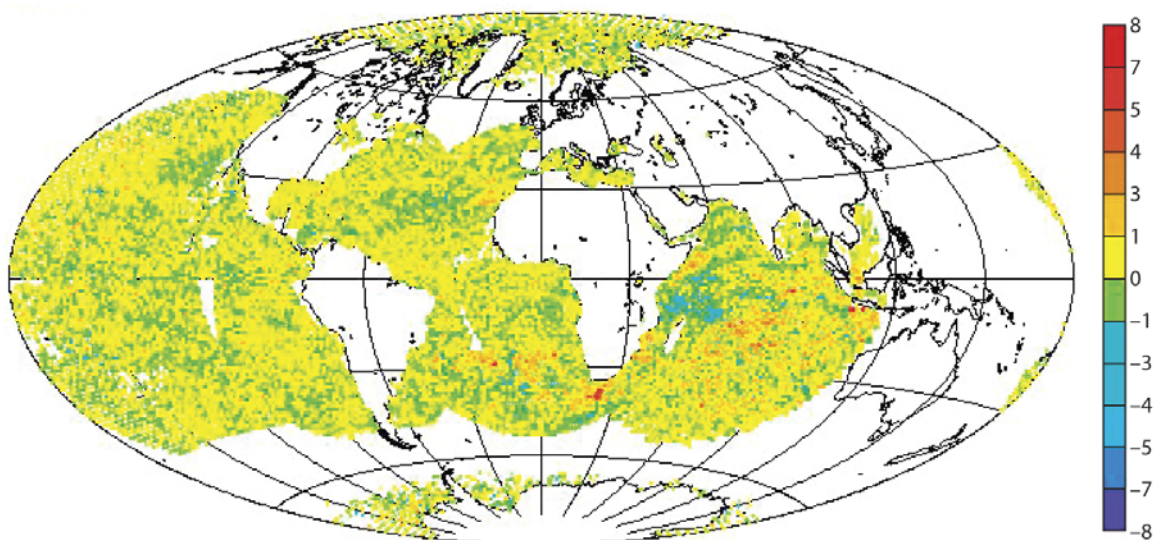


Figure 3: 00 UTC forecast error contribution (J/kg) (third order sensitivity gradient) of the observed u -component of the wind between 700 and 1000 hPa from GOES and METEOSAT visible wavelength bands accumulated over one month in summer 2006. Negative (positive) values correspond to a decrease (increase) of forecast error.

The impact of AMVs on the forecast has also been assessed through the OSE. Among the different OSEs performed at ECMWF, one in particular was performed to measure the impact of assimilated AMVs by comparing the *reference* experiment (all conventional observations plus AMSU-A radiances from NOAA-16) with an experiment containing AMV observations in addition to the observations used in *reference* (see Table 2). Figure 4 shows the *rms* (root mean square) forecast error differences between Reference and AMV experiments for the 24-hour forecast starting at 00 UTC for the 850 hPa u-wind component. Similar degradation appears in area-1, area-2 and area-3 defined above. The largest degradation in the South Pacific (Figure 4) is supported to a lesser extent by FSO diagnostic (Figure 3).

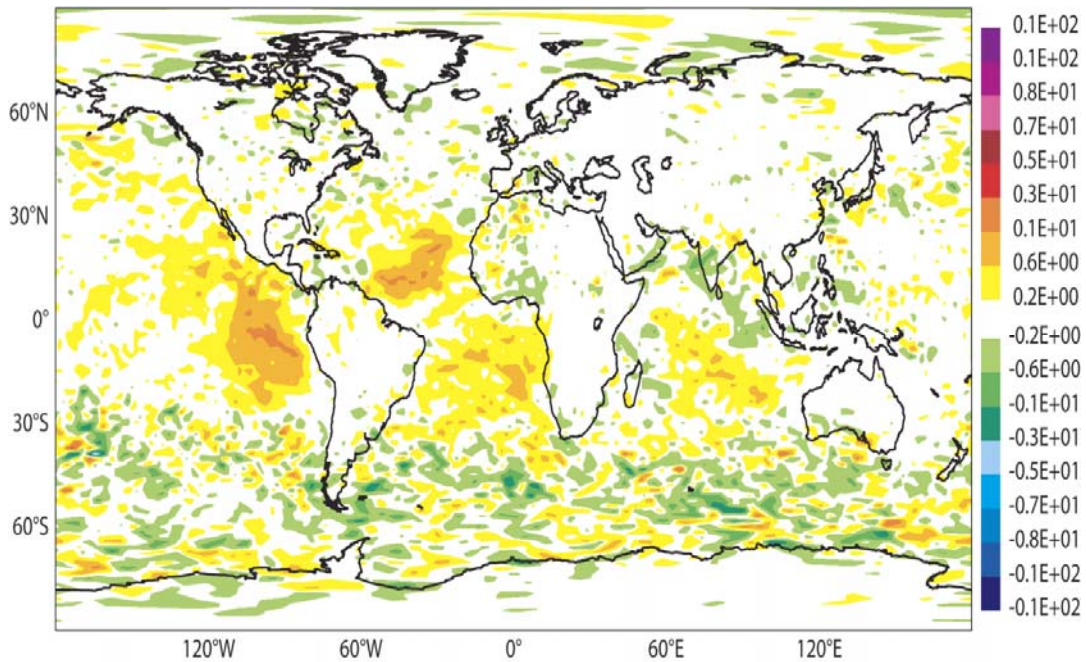


Figure 4: rms forecast error differences between AMV and Reference OSEs of the 24 hour forecast starting at 00UTC for the u-component of the wind at 850 hpa (m/s). Positive (negative) contours indicate AMV errors are larger (smaller) than Reference errors.

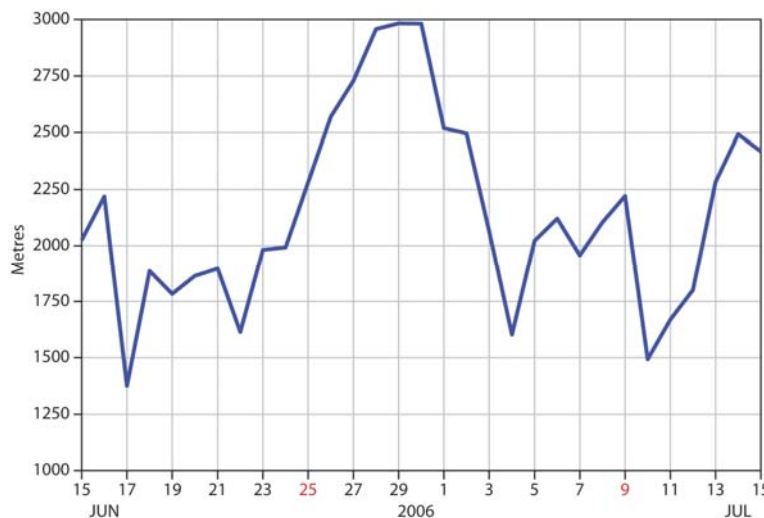


Figure 5 Time series of averaged boundary layer top height from 21-hour forecasts valid at 15:00 local time of all American wind profile stations over the summer period.

Figure 1 shows also a forecast error increase due to PILOT observations (Table 1). The geographical display of the forecast error for PILOT observations (not shown) indicates that the degradation was coming from the American wind profilers. Problems with the American wind profilers at low levels (below 700 hPa) were known in spring time due to bird migration contamination (Wilczak *et al.* 1995). But other meteorological situations also produce a contamination of profiler measurements (Ackley *et al.* 1998), one of which is the limitation of the local horizontal atmospheric uniformity assumption that must be satisfied to have a correct mean wind measure. Meteorological conditions in which short spatial and temporal scales of variability have amplitudes as large as the mean, as for example in the presence of a CBL (Convective Boundary Layer) and severe storms, limit the horizontal wind measurement. It was effectively found that the CBL-activity was rather high for this period as can be see from the large height of the boundary layer at the station locations, averaged among all profiler stations (Figure 5).

It was also found that both CAPE and TCWV compared with the ERA climatology (Uppala *et al.* 2005) indicated larger CAPE and humidity advection from the Gulf of Mexico in areas where wind profilers are located (not shown). Together, high TCWV and CAPE, triggered the convection activity. The lessons learnt with wind profilers is that their impact on the forecast can change quite a lot given the meteorological situations, therefore monitoring their impact on forecast skill, on a daily basis, would allow a more efficient screening of the contaminated measurements.

3.1.2 Winter

The winter period examined in this paper ranges from 5 January to 12 February 2007. On the 24-hour forecast error the global observation performance (Figure 9) is very similar to the summer one shown in Figure 1. Again some forecast skill deteriorations are produced by METEOSAT and GOES AMVs obtained from the visible and infrared band and to a lesser extent from GPS-RO (Global Positioning System satellite Radio Occultation). Impact studies on the use of GPS-RO observations had shown a positive impact in the forecast (Healy and Thépaut 2006) at different ranges with the exception of the 24-hour forecast range (Figure 6). The OSE was performed by removing the GPS-RO observations (GPSRO experiment) from the operational data set (Table 2). Figure 6 shows the *rmse* of the temperature field at 50 hPa (about 20 km) in the tropical band for GPSRO (solid line) and *control* (dashed line) experiment (assimilating the full operational observation set) for the same winter period. On the 24-hour forecast the impact of GPS-RO data is negative (Figure 6) becoming positive only past the 48-hour forecast range. Figure 7 shows the forecast error contribution of GPS-RO measurements at different vertical levels (distance in km from the surface) for the 24-hour. The large detrimental effect on the 24 hour forecast accuracy is observed from 100 hPa upwards (above 17 km, Figure 7a), geographically, the increase of forecast error is more pronounced at tropical and subtropical latitudes (not shown).

The comparisons with the OSE clearly indicate that the FSO diagnostic highlights already at the first screening (see for example Figure 1 or 9) the major forecast degradation due to the observations. FSO provides similar qualitative diagnostic picture as the observing system experiments, but by using OSE, more difficulties are encountered to identify the regions or the vertical level of the problem. According to OSE, GPSRO performs better than *control* only after day 2, and the improvement increases with forecast range (up to 0.3 degree in temperature at day 10). Results produced with 48 hour FSO (not shown) confirmed that at this range GPS-RO observations have a positive impact in the forecast, suggesting therefore that the negative impact substantially depends on the verifying analysis used to compute the forecast error. In the future, a

different objective function where the forecast error is computed by comparing the forecast with independent observation is planned to be also used.

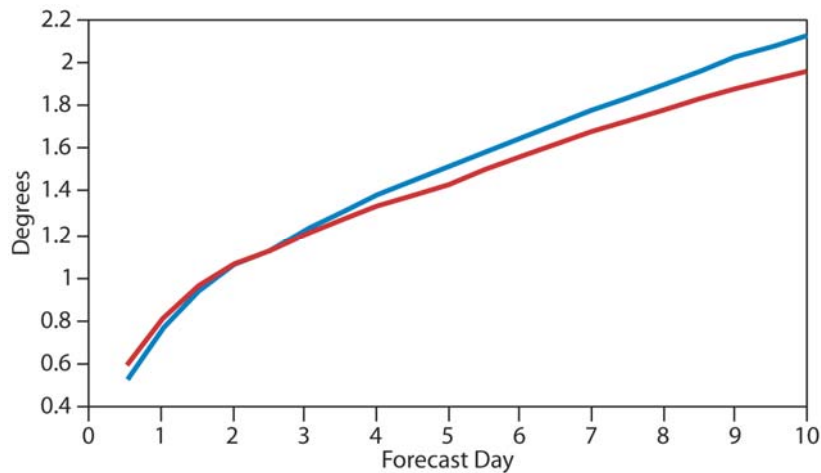


Figure 6: 50 hPa rmse of one month of temperature field at 50 hPa in the tropics for GPSRO (solid line) and control (dashed line) experiments versus forecast length.

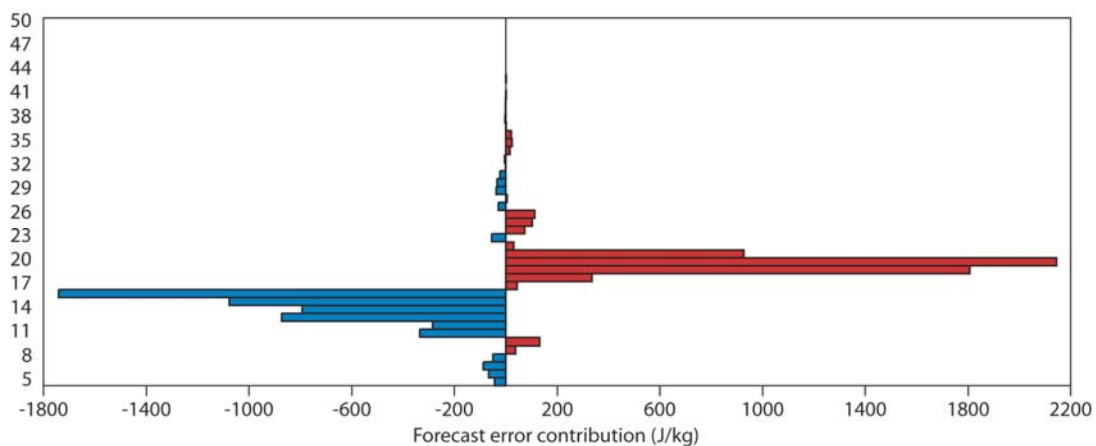


Figure 7: 24 hour Forecast error contribution (third order sensitivity gradient) of GPS-RO at different vertical levels, from 5 km to the surface up to 50 km.

SYNOP surface pressure observations that are globally decreasing the forecast error (see Figure 9), nevertheless have a negative impact over Europe (not shown). Further investigation showed that a group of land stations over Germany and France were persistently increasing the forecast error. A persistent north-westerly flow occurred over Europe for three weeks, which entailed strong near-surface pressure variations. The sea surface pressure ranged from 8 hPa below average in north Germany and England to 4 hPa above in South of Italy. The comparisons between observation and background (observation departure) indicate that manual SYNOP station had a positive bias (12 Pa, Figure 8 top-left panel) which was halved after the minimization (5 Pa, Figure 8 top-right panel). On the contrary, automatic land stations (METAR) were, on the monthly average, measuring lower surface pressures (-30 Pa) than the model background (Figure 8 bottom-left panel) and the negative bias increased after the minimization (Figure 8 bottom-right panel, -35 Pa) showing that the analysis solution was not found in the direction of deeper surface pressure measurements. Interestingly, the increase of forecast error was due to the stations that were instead measuring higher pressure than the background. The weather situation was such that the strong surface

pressure gradient (over the entire month) generated, in that area, a large spread of pressure measurements (not shown) that was not represented in the model at the used resolution. In the minimization procedure the direction towards those observations that were measuring higher pressure than the background was selected providing, later on, a negative impact in the forecast.

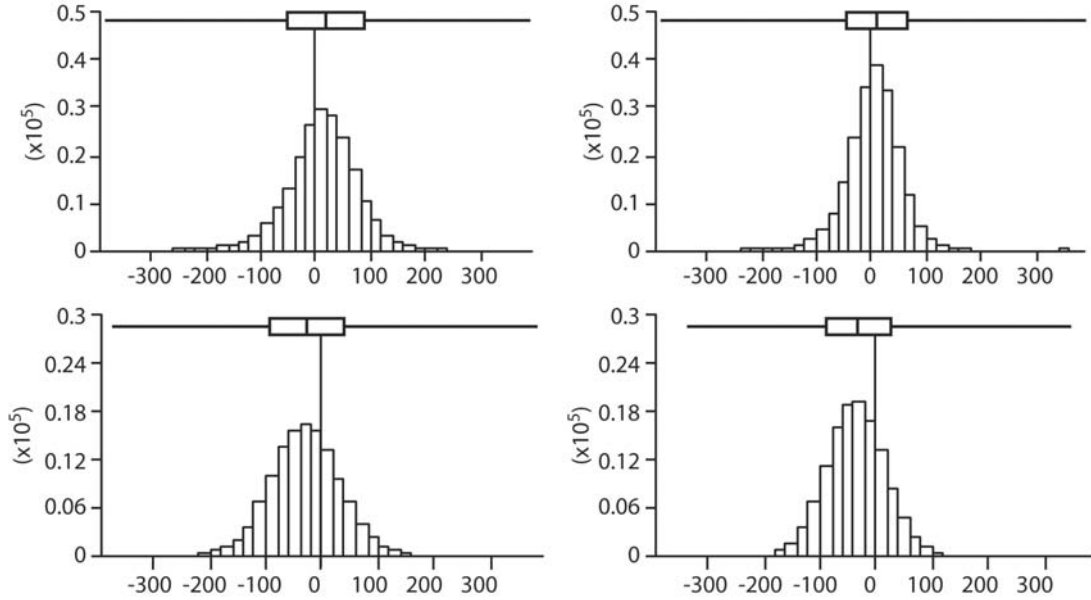


Figure 8 Surface pressure observation minus first guess (left panel) and observation minus analysis (right panel) for the winter period and for the SYNOP stations in the area of forecast degradation. SYNOP manual (upper panel) and SYNOP METAR (bottom panel) show large opposite bias.

3.2 First order sensitivity gradient

Now compare the first order sensitivity gradient with the third order one. On this subject, let $J_1(\mathbf{e}) = \|\mathbf{e}, \mathbf{C}\mathbf{e}\|$ express the variation in the forecast error due to the assimilation of observations, which is $J(\mathbf{e}_a) - J(\mathbf{e}_b)$ where the \mathbf{e}_a and \mathbf{e}_b are the analysis and the background error. Following Langland and Baker, the second (or third) order Taylor series decomposition (see also Errico 2007) is used to map such variation

$$J(\mathbf{e}_b) - J(\mathbf{e}_a) = (\mathbf{e}_b - \mathbf{e}_a)^T J'_{e_a} + \frac{1}{2} (\mathbf{e}_b - \mathbf{e}_a)^T J''_{e_a} (\mathbf{e}_b - \mathbf{e}_a) \quad (3.1)$$

Because the error cost function is quadratic, (3.1) reduces to

$$J(\mathbf{e}_b) - J(\mathbf{e}_a) = 2(\mathbf{e}_b - \mathbf{e}_a)^T \mathbf{e}_a + (\mathbf{e}_b - \mathbf{e}_a)^T (\mathbf{e}_b - \mathbf{e}_a) \quad (3.2)$$

which at the first order is

$$J(\mathbf{e}_b) - J(\mathbf{e}_a) = -2\mathbf{d}^T \mathbf{K}^T \mathbf{e}_a \quad (3.3)$$

In an optimal assimilation system, the right hand side of the equation is on average zero (Talagrand, 2002) since statistically, the innovation vector, $\mathbf{d} = \mathbf{y} - \mathbf{H}\mathbf{x}_b$, and the analysis error are orthogonal. The results obtained by using the first order sensitivity gradient, only provides the measure of the sub-optimality of the analysis system. Therefore, the second order term appears necessary to be included in the FSO calculation.

Experiments (summer and winter) were also performed by using a first order sensitivity gradient. Figure 9 shows the FSO from 24 hour first order sensitivity gradient (left panel) and from 24 hour third order

sensitivity gradient (right panel). It is clear that quantitatively the diagnostic based on a different order gradient is very different (almost a factor 3) for all the observation types.

For the first order gradient, global negative impact is also noticed from radiance data for GOES and Meteosat, from AMSU-B and from AMV for GOES in the infrared band. Also, the negative impact of GPS-RO is larger when first order sensitivity gradient are used. A further comparison is shown for the SCAT data v-components (Quikscat and ERS instruments). Figure 10 shows the global distribution of the forecast error

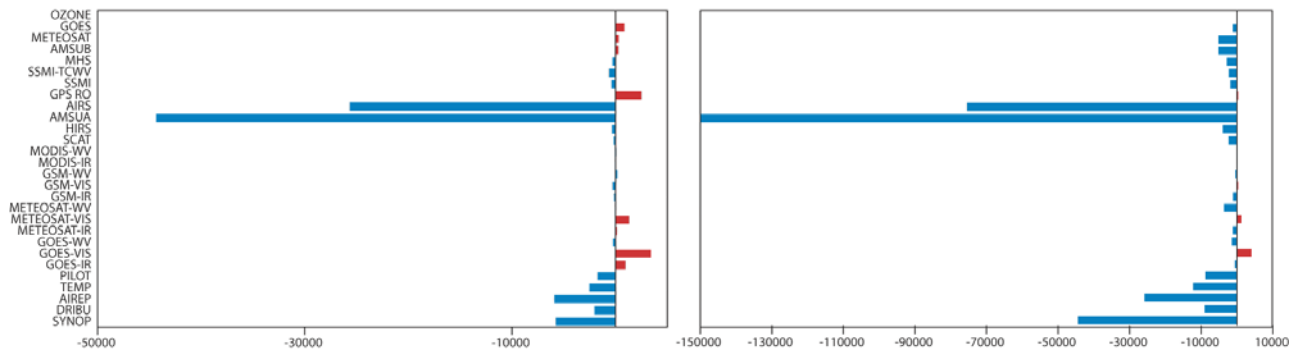


Figure 9 24-hour forecast error contribution in J/kg of the components (types) of the observing system in winter 2007. Negative (positive) values correspond to a decrease (increase) in the energy norm of forecast error. Left panel FSO uses a first order sensitivity gradient and right panel a third order sensitivity gradient.

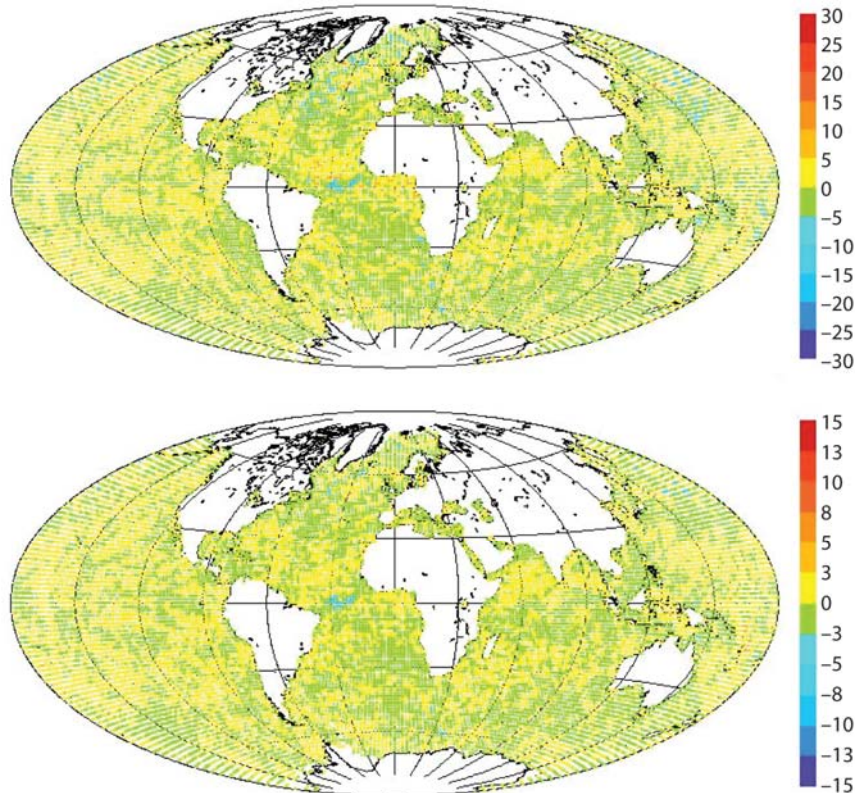


Figure 10 Forecast error contribution at 00 UTC (J/kg) of the observed v-component of the wind from ERS and Quikscat scatterometers. Negative (positive) values correspond to a decrease (increase) of forecast error. Bottom panel FSO_{24}^{1stO} and top panel FSO_{24}^{3rdO} .

contribution at 00 UTC for the winter period for the FSO_{24}^{1stO} (first order, bottom panel) and FSO_{24}^{3rdO} (third order, top panel) below 900 hPa. The FSO_{24}^{1stO} values are less than half the FSO_{24}^{3rdO} values but the geographical pattern of positive and negative values is quite similar, e.g. over the tropical band, in particular at the equator over the Atlantic ocean; for the extra-tropics, in particular in the Northern Hemisphere over the Pacific. The SCAT OSE diagnostic also shows, on the 24 hours forecast range, similar degradation for the v-component below 900 hPa in terms of *rmse* differences between SCAT and *reference* (not shown). The pattern similarity of the variation of the forecast error between the first and the third order sensitivity gradient is also observed for some other data types mainly satellite data which indicates that the causes are related with the analysis performance, in particular the sub-optimality of the analysis system.

4 Performance of the ECMWF operational model

In this section, the overall impact of the operational observation network on the forecast is illustrated. The forecast is computed at T511 resolution (T799 operationally) consequently T511TL255L91 is the FSO resolution used. The assimilation and forecast system are the operational (CY35R2). The investigated period is from September to December 2008. Figure 11 shows the total impact over the four months of the different components of the observation network on the 24-hour forecast. The impact is expressed in terms of variation of the forecast error, positive values mean the forecast error is increased, and negative values indicate that the forecast error is decreased due to a particular observation type. Overall, the observations all contribute to decrease the forecast error (Figure 11 $\text{Joule} \times 10^{-4}$). Ozone observations have a neutral impact. The largest contribution is provided by AMSU-A data, followed by IASI and AIRS. Among the conventional observations AIREP (aircraft data) have the most positive impact comparable with GPS-RO that shows a considerable improvement with respect to the previous results (model cycle CY31R2). Noticeable is also the impact of radiosonde and surface pressure observations (TEMP, SYNOP and DRIBU). Larger impact is also found for SCAT data and the performance of METEOSAT and GOES geostationary wind measurements is improved as well. The previous results were based on only 1 month (2 different seasons) for 2006 and 2007, the most recent results (4 months end of 2008) use more observations, for example GPS-RO are 8 times more numerous (65 million of measurements) than in 2007.

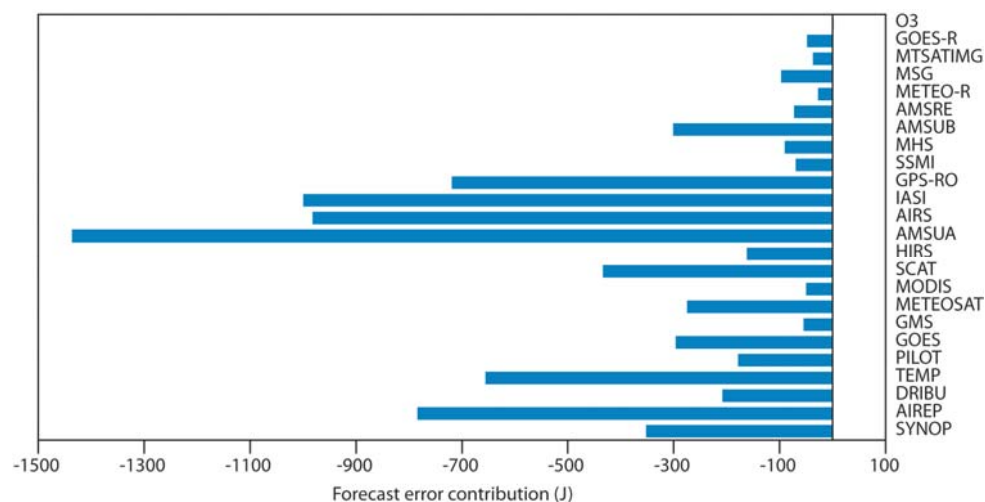


Figure 11. 24-hour forecast error contribution ($\text{Joule} \times 10^{-4}$) of the components (types) of the observing system during September, October, November and December 2008. Negative (positive) values correspond to a decrease (increase) in the energy norm of forecast error.

The overall larger and positive impact of all the currently assimilated observations on the short-range forecast also provides a clear indication that from 2006 to 2009 the assimilation and forecast system have improved.

In Figure 13 the forecast error contribution of AIRS data is shown per channel assimilated. The most neutral results are found from channels 305 to 843 sensitive to temperature and water vapor with maximum sensitivity at 850 hPa. Similar neutral impact is found for IASI (Figure 14) from channel 16 to 191 that peek at around 50-100 hPa sensitive to temperature, and from channel 366 to 921 sensitive to water vapor at 800 hPa and temperature at 950 hPa. The performance of GPS-RO observations is quite impressive at all levels. The number of observation per level is similar, but the distribution of forecast error contribution is quite symmetrical around 14 km from the surface (Figure 14). The distribution mimics the observation influence given in the analysis to radio occultation measurements at different levels in the atmosphere (not shown).

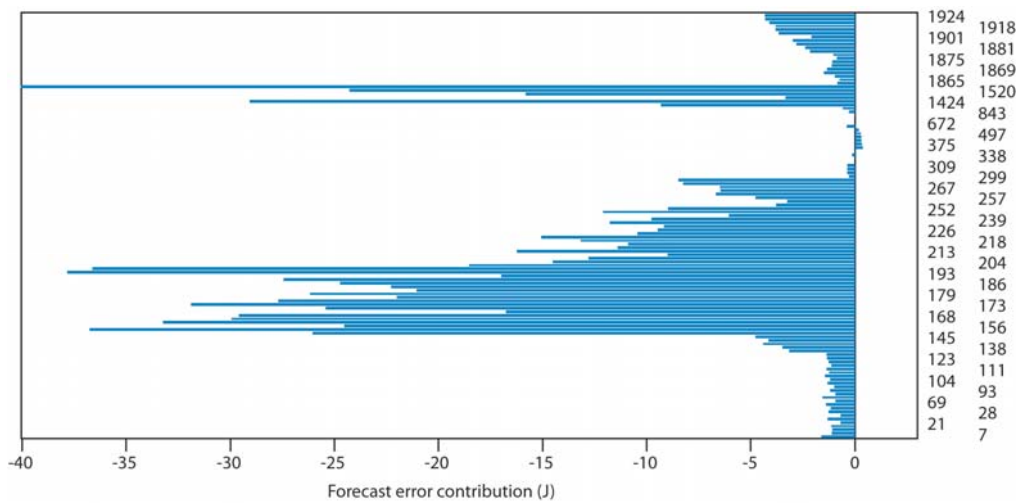


Figure 12. 24-hour forecast error contribution (Joule*10⁻⁴) of AIRS with respect to all the assimilated channels during September, October, November and December 2008. Negative (positive) values correspond to a decrease (increase) in the energy norm of forecast error.

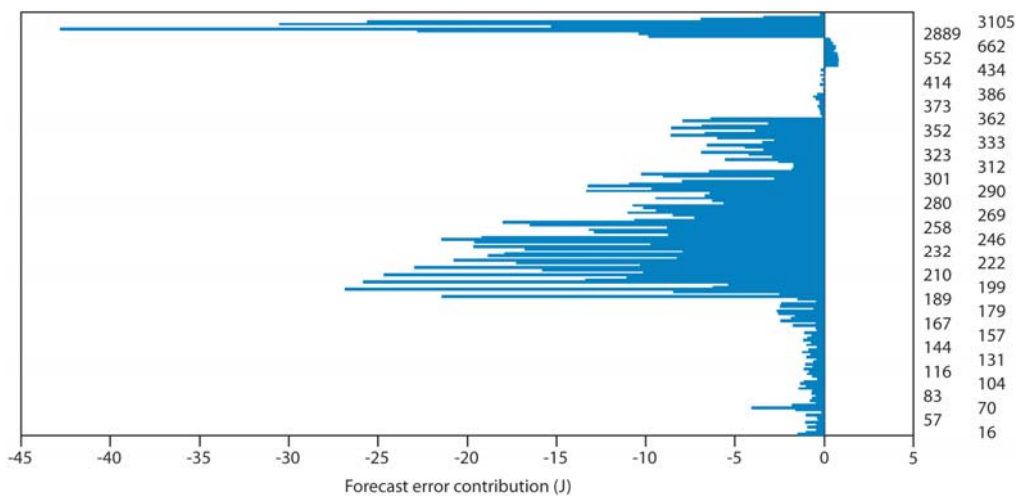


Figure 13. 24-hour forecast error contribution (Joule*10⁻⁴) of IASI with respect to all assimilated channels during September, October, November and December 2008. Negative (positive) values correspond to a decrease (increase) in the energy norm of forecast error.

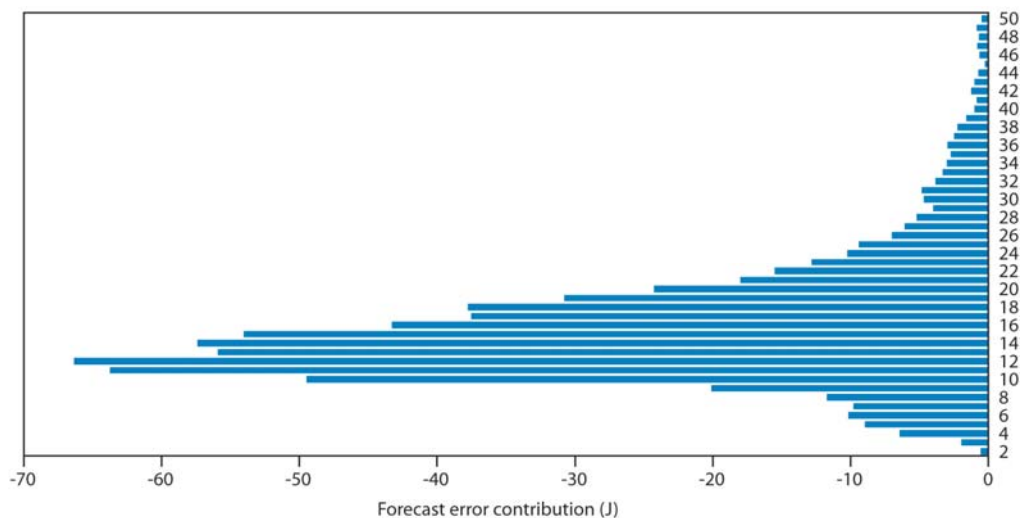


Figure 14: 24 hour Forecast error contribution (Joule*10⁻⁴) of GPS-RO at different vertical levels, from 2 km above the surface up to 50 km.

Recent changes applied to the assimilation of GPS-RO data include the reduction of the observation error standard deviation and the extended usage on the vertical up to 50 km. Also in 2006, GRAS was not used and the number of data from this satellite counts for almost one third of the total radio occultation measurements amount.

For a complete understanding of the plot diagrams shown, a significance test or error bars of the impact measure will be computed. A consistent statistical sample of forecast error contribution from all observation type and all over different seasons and months of the year need to be gathered. Anyhow, it should be kept in mind that with the 16% limit of the FSO solution accuracy, small negative or positive values are regarded as neutral impact.

5 Conclusions

Over the last few years, the potential of using derived adjoint-based diagnostic tools has been increasingly exploited. Recently, a compact derivation of the 4D-Var sensitivity equations by using the theoretical framework of the implicit function has been derived (Daescu 2008). The analytical formulation of the sensitivity equations with respect to an extended set of input parameters has been shown and numerical applications will soon follow. This paper illustrates the use of the forecast sensitivity with respect to time-distributed observational data, first time in a 12-hour 4D-Var assimilation system, as a diagnostic tool to monitor the observation performance in the short-range forecast.

Here, the forecast sensitivity to the observation has been based on the forecast error of the *control* experiment from observing system experiments that have been performed at ECMWF, with the intention of comparing the performance of the two diagnostic tools. The assessment of the value of observations for forecast error reduction through the OSEs is performed by comparing the forecast skill obtained with and without the subset of data of interest. This usually involves large numbers of independent experiments over several months and is therefore quite expensive to perform and prohibitive if a detailed investigation of operational observing systems must be obtained. Also, any variation in the observation set that is assimilated through data addition or data denial modifies the Kalman gain matrix, producing therefore different solutions

in the minimization. However, observation forecast impact on the medium and long-range can also be investigated.

Forecast sensitivity to observations can only be used to diagnose the impact on the short-range forecast, namely 24 to 48 hours, given the use of a simplified adjoint of the data assimilation system and the implied linearity assumption. On the other hand, the use of FSO allows the identification of potential problems and directs further investigations. It was demonstrated that, on the short-range forecast, FSO and OSE provide a very similar qualitative picture of improvement or degradation due to observations. The forecast degradation that was observed at certain pressure levels and in a number of areas in the OSE due to some observation type, matches well with the FSO forecast error contribution maps for the same observation type. Clearly, the two tools have different meaning of use. Whilst OSEs are more indicated for evaluating the longer term forecast impact of data, FSO should be used to investigate the reasons of short-range forecast failure due to the misuse of observations. Furthermore, FSO allows further granularity in the investigation (observation type, level, channel, etc.) at no extra cost.

It was found that it is necessary to use the third order sensitivity gradient to fully document the forecast impact from the observations. The first order only represents the sub-optimality of the assimilation system. Quantitatively the results from the two different orders of gradients are quite different, first the forecast error variation is three times smaller for the first order than the third order and second, the negative impact of some observation type, as GOES and Meteosat radiances and atmospheric motion vectors, is only present when the first order gradient is used. Nevertheless, comparison on pattern variation of forecast error contribution shows quite large similarities for some data type, for example for the satellite motion vectors and the scatterometer data, which indicates that the short-range observation forecast impact is affected by the sub-optimality of the analysis system. It highlights the importance of performing an efficient monitoring of the assimilation system to objectively determine if the given scheme is optimal in terms of 'best linear and unbiased estimate' of the initial condition from all information available (Talagrand, 1999).

Over the two months period, the global impact of observations was found to be positive and the forecast errors decrease for almost all data type. Problems have been noticed with Atmospheric Motion Vectors mainly derived from visible and infrared wavelength bands (and for low-level winds). Problems with conventional observations, wind profilers in summer and SYNOP Metar surface pressure observations in winter, was mainly due, for different reasons, to the local synoptic situation. Wind profiler measurements were corrupted by the presence of strong convection activity in the boundary layer, while large surface pressure variability that characterized the entire winter month at the surface over the small domain of eastern France and Germany, was not correctly solved in the minimization.

Over the most recent four months period examined in autumn 2008, the impact of all types of observations on the short-range forecast has increased impressively. It has been shown that microwave satellite measurements (AMSU-A) are responsible for 18% of the forecast error reduction, infrared measurements (AIRS and IASI) for 12% and 10% of error reduction is due to radio occultation observations. Conventional observations (surface pressure, vertical profiler and aircraft) are as well decreasing the forecast error, being responsible for an average reduction of 6%. A statistical significance of the observation impact will be soon added once a robust statistical sample of these diagnostics is provided.

Given the dependency of some observation types on the meteorological situation, it is suggested to run the forecast sensitivity to the observation diagnostic tool on an operational basis and in relation to the operational suite error. A constant monitoring of the performance of the model forecast would allow the use of the observation network in an adaptive way where situations with negative observation impact can be investigated and improved or potentially denied in real time.

FSO is ready to be implemented. Improvements to the forecast error calculation by directly comparing forecast fields with observations instead of analysis fields are continuing. It will better highlight the problems related to bias, helping thus to distinguish between biases in the model or in the observations.

6 References

- Ackley M., R. Chadwick J. Cogan, C. Crosiar, F. Eaton, K.Gage, E. Gossard, R. Lucci, F. Merceret, W. Neff, M. Ralph, R. Strauch, D. Van de Kamp, B. Weber, A. White, 1998: U.S. Wind Profilers: A review. FCM-R14-1998
- Andersson, E. and Fisher, M. 1999: Background errors for observed quantities and their propagation in time. Proc. ECMWF Workshop on “Diagnosis of Data Assimilation Systems”, Reading, U.K., 1-4 Nov. 1998, 81—90.
- Baker N.L. and R. Daley, 2000: Observation and background adjoint sensitivity in the adaptive observation targeting problem. *Q. J. R. Meteorol. Soc.*, **126**,1431-1454
- Bormann, N., Saarinen, S., Kelly G. and Thépaut, J-N. 2003: The spatial structure of observation errors in atmospheric motion vectors from geostationary satellite data. *Mon. Wea. Rev.*, **131**, 706—718.
- Bouttier, F, and Kelly, G., 2001: Observing system experiments in the ECMWF 4D-Var data assimilation system. *Q. J. R. Meteorol. Soc.*, **127**,1469-1488
- Cardinali, C., S. Pezzulli and E. Andersson, 2004: Influence matrix diagnostics of a data assimilation system. *Q. J. R. Meteorol. Soc.*, **130**, 2767—2786
- Cardinali, C., and R. Buizza: 2004. Observation sensitivity to the analysis and the forecast: a case study during ATreC targeting campaign. Proceedings of the First THORPEX International Science Symposium, 6-10 December 2004, Montreal, Canada, WMO TD 1237 WWRP/THORPEX N. 6.
- Chapnik, B., G.Desnozier, F. Rabier and O. Talagrand, 2006: Diagnosis and tuning of observation error in a quasi-operational data assimilation setting. *Q. J. R. Meteorol. Soc.*, **132**, 543—565.
- Courtier P., E. Andersson, W. Heckley, J. Pailleux, D. Vasiljevic, M. Hamrud, A. Hollingsworth, F. Rabier and M. Fisher, 1998: The ECMWF implementation of three-dimension variational assimilation (3D-Var). Part I: Formulation. *Q. J. R. Meteorol. Soc.*, **124**, 1783—1807
- Daescu, D.N., 2008: On the sensitivity equations of 4D-Var data assimilation. *Mon. Wea. Rev.*, accepted for publication.

- English, S., R. Saunders, B. Candy, M. Forsythe, and A. Collard, 2004: Met Office satellite data OSEs. Third WMO Workshop on the impact of various observing systems on numerical weather prediction, Alpbach, Austria, WMO/TD, **1228**, 146-156
- Errico, R., 2007: Interpretation of an adjoint-derived observational impact measure. *Tellus*, **59A**, 273-276.
- Fisher, M., 1996: The specification of background error variances in the ECMWF variational analysis system. Proc. ECMWF workshop on “Non-linear aspects of data assimilation”, Reading, 9-11 September 1996, 645—652.
- Fisher, M., 2003: Estimation of entropy reduction and degrees of freedom for signal for large variational analysis systems. *ECMWF Tech. Memo.*, **397**, pp 18.
- Fisher, M. and Courtier, P., 1995: Estimating the covariance matrices of analysis and forecast error in variational data assimilation. *ECMWF Tech Memo.*, **220**, pp 26.
- Fisher, M. and Andersson, E., 2001: Developments in 4D-Var and Kalman Filtering. *ECMWF Tech Memo.*, **347**, pp 36.
- Fourrié, N. and Thépaut, J-N., 2003: Evaluation of the AIRS near-real-time channel selection for application to Numerical Weather Prediction. *Q. J. R. Meteorol. Soc.*, **129**, 2425-2439.
- Gelaro R, Buizza, R., Palmer T.N. and Klinker E., 1998: Sensitivity analysis of forecast errors and the construction of optimal perturbations using singular vectors. *J. Atmos. Sci.*, **55**, 1012—1037.
- Healy, S., and J-N. Thépaut, 2006: Assimilation experiments with CHAMP GPS radio occultation measurements. *Q. J. R. Meteorol. Soc.*, **132**, 605-623.
- Isaksen L., M. Fisher, E. Andersson, and J. Barkmeijer 2005: The structure and realism of sensitivity perturbations and their interpretation as 'Key Analysis'. *Q. J. R. Meteorol. Soc.*, **131**, 3053—3078.
- Janiskova, M., J.-J. M. J.-F. Mahfouf, and F. Chevallier, 2002: Linearized radiation and cloud schemes in the ECMWF model: Development and evaluation, *Q. J. R. Meteorol. Soc.*, **128**, 1505—1527.
- Kelly, G., and Thépaut, J-N 2007: Evaluation of the impact of the space component of the Global Observation System through Observing System Experiments. ECMWF Newsletter No 113, 16-28.
- Langland R. and N.L Baker., 2004: Estimation of observation impact using the NRL atmospheric variational data assimilation adjoint system. *Tellus*, **56A**, 189-201.
- Lorenc, A., 1986: Analysis methods for numerical weather prediction. *Q. J. R. Meteorol. Soc.*, **112**, 1177—1194.
- Lopez, P. and E. Moreau, 2005: A convection scheme for data assimilation: Description and initial tests. *Q.J.R.Meteorol.Soc.*, **131**, 409—436

- Lord, S., T. Zapotocny, and J. Jung, 2004: Observing system experiments with NCEP's global forecast system. Third WMO Workshop on the impact of various observing systems on numerical weather prediction, Alpbach, Austria, WMO/TD, **1228**, 56-62.
- Purser, R. J. and Huang, H.-L., 1993: Estimating Effective Data Density in a Satellite Retrieval or an Objective Analysis. *J. Appl. Meteorol.*, **32**, 1092—1107.
- Rabier, F. and Courtier, P., 1992: Four-dimensional assimilation in the presence of baroclinic instability. *Q. J. R. Meteorol. Soc.*, **118**, 649—672.
- Rabier, F., Klinker, E., Courtier, P. and Hollingsworth A. 1996: Sensitivity of forecast errors to initial condition. *Q. J. R. Meteorol. Soc.* **122**, 121—150
- Rabier, F., Järvinen, H., Klinker, E., Mahfouf J.F., and Simmons, A., 2000: The ECMWF operational implementation of four-dimensional variational assimilation. Part I: experimental results with simplified physics. *Q. J. R. Meteorol. Soc.* **126**, 1143—1170.
- Talagrand, O., 1997: Assimilation of observations, an Introduction. *J. Meteorol. Soc. Japan*, **Vol 75**, N.1B, 191—209.
- Talagrand, O., 1999: A posteriori evaluation and verification of the analysis and assimilation algorithms. Proceedings of Workshop on diagnosis of data assimilation systems, ECMWF, Reading, England.
- Talagrand O., 2002: A posteriori validation of assimilation algorithms. Proceeding of NATO Advanced Study Institute on Data Assimilation for the Earth System, Acquafreda, Maratea, Italy.
- Thépaut, J.N., Hoffman, R.N. and Courtier, P., 1993: Interactions of dynamics and observations in a four-dimensional variational assimilation. *Mon. Wea. Rev.*, **121**, 3393—3414.
- Thépaut, J.N., Courtier, P., Belaud G. and Lemaître, G., 1996: Dynamical structure functions in four-dimensional variational assimilation: A case study. *Q. J. R. Meteorol. Soc.*, **122**, 535—561.
- Tompkins, A.M. and M. Janiskova: 2004, A cloud scheme for data assimilation: Description and initial tests. *Q.J.R.Meteorol.Soc.*, **130**, 2495—2517
- Uppala, S.M., Kållberg, P.W., Simmons, A.J., Andrae, U., da Costa Bechtold, V., Fiorino, M., Gibson, J.K., Haseler, J., Hernandez, A., Kelly, G.A., Li, X., Onogi, K., Saarinen, S., Sokka, N., Allan, R.P., Andersson, E., Arpe, K., Balmaseda, M.A., Beljaars, A.C.M., van de Berg, L., Bidlot, J., Bormann, N., Caires, S., Chevallier, F., Dethof, A., Dragosavac, M., Fisher, M., Fuentes, M., Hagemann, S., Hólm, E., Hoskins, B.J., Isaksen, L., Janssen, P.A.E.M., Jenne, R., McNally, A.P., Mahfouf, J.-F., Morcrette, J.-J., Rayner, N.A., Saunders, R.W., Simon, P., Sterl, A., Trenberth, K.E., Untch, A., Vasiljevic, D., Viterbo, P., and Woollen, J. 2005: The ERA-40 re-analysis. *Q. J. R. Meteorol. Soc.*, **131**, 2961—3012.
- Van der Vorst, H.A., 2003: Iterative Krylov methods for large linear systems. *Cambridge Accademic Press*

Wilczak, J., R. Strauch, F. Ralph, B. Weber, D. Merritt, J. Jordan, D. Wolfe, L. Lewis, D. Wuertz, J. Gaynor, S. McLaughlin, R. Rogers, A. Riddle, and T. Dye, 1995: Contamination of Wind Profiler Data by Migrating Birds: Characteristics of Corrupted Data and Potential Solutions. *J. Atmos. Oceanic Technol.*, **12**, 449-467.

WMO, 1996: Guide to meteorological instruments and methods of observation. Sixth Edition. WMO-No.8. Geneva, Switzerland.

Zhu, Y. and Gelaro, R., 2008: Observation Sensitivity Calculations Using the Adjoint of the Gridpoint Statistical Interpolation (GSI) Analysis System. *Mon. Wea. Rev.*, **136**, 335—351.

Appendix A

The results of a different response function can be examined in order to measure the accuracy of the solution in (2.10). Let define $J_{test} = \frac{1}{2} \langle \delta \mathbf{x}_a, \delta \mathbf{x}_a \rangle$. The gradient of J_{test} with respect to $\delta \mathbf{x}_a$ is the analysis increments themselves, then (2.11) becomes

$$\delta J_{test} = \left\langle \frac{\partial J_{test}}{\partial \mathbf{x}_a}, \delta \mathbf{x}_a \right\rangle = \langle \delta \mathbf{x}_a, \delta \mathbf{x}_a \rangle = \left\langle \frac{\partial J_{test}}{\partial \mathbf{y}}, \delta \mathbf{y} \right\rangle = \delta J_{test}^{computed} \quad (\text{A.1})$$

It is clear that, although the response function is not of meteorological significance, it has the convenience that its gradient is equivalent to the increments themselves and their scalar product is exactly computed.

The solution accuracy is therefore defined as

$$\frac{\delta J_{test}^{computed} - \delta J_{test}}{\delta J_{test}}$$

In Table A.1 the accuracy of the solution, in percentage, is shown for different observation types and FSO (Forecast Sensitivity to Observation) experiment set-up compared with the AN (Analysis) experiment set-up from which the forecast error is computed.

Table A.3 FSO accuracy with respect to the observation used and the configuration adopted

AN	FSO	Observation Assimilated	Type	Observed Parameter	Observation Number	Solution Accuracy %
T159TL159	T159TL159	Radiosonde		T	24556	-0.0004
T159TL159	T159TL159	Radiosonde		U, V	42710	0.007
T159TL159	T159TL159	SYNOP DRIBU		ps	92410	-17.8
T159TL159	T159TL159	GPS-RO		Bending Angle	296209	0.06
T159TL159	T159TL159	Satellite		Radiance	8163313	17.9
T159TL159	T159TL159	All		All	9156768	16
T511TL159	T511TL159	All		All	9247733	16
T511TL95TL159TL255	T511TL255	All		All	9237743	16.7
T511TL95TL159TL255 GPINNER=true	T511TL255 GPINNER=false	All		All	9237743	16.7
T511TL95TL159TL255 GPINNER=true	T511TL255 GPINNER=false	All-SYNOP&DRIBU		All-ps	9145333	16.8

The accuracy depends on the observation type: surface pressure observations have the lowest accuracy (-17%) together with satellite radiances data whilst a very good accuracy is shown for conventional radiosonde observation either for the u and v component of the wind or temperature and for GPS Radio-Occultation (less than 0.06%). However, when all the observations are assimilated the total accuracy converge to 16% for the same AN and FSO configuration set-up, that is, same resolution for the inner and outer loop and only one inner loop performed. A very small degradation (less than 1%) is added when AN has more number of inner

loops with respect to FSO. In particular, in the AN configuration (operational configuration) three different minimization (multi-incremental 4D-Var) loops at TL95, TL159 and TL255 spectral truncation are performed, whilst FSO solves in one go the linear equation system at the higher resolution TL255. The last difference between the two configurations comes from the numerical representation of the humidity field: the AN operational configuration handles the humidity variable on a Gaussian grid (logical switch GPINNER=true) during the non-linear, tangent linear and adjoint integration whilst due to the sensitivity gradient present form computation, FSO handles spectral representation of the humidity variable (GPINNER=false). However, the difference above explained does not change the FSO solution accuracy. The solution accuracy of 17% is a quite satisfactory result, it allows both a qualitative and quantitative assessment of the forecast impact.

Appendix B

FSO *sms* (logical computational diagram) pre-operational configuration is presented in Figure B1.

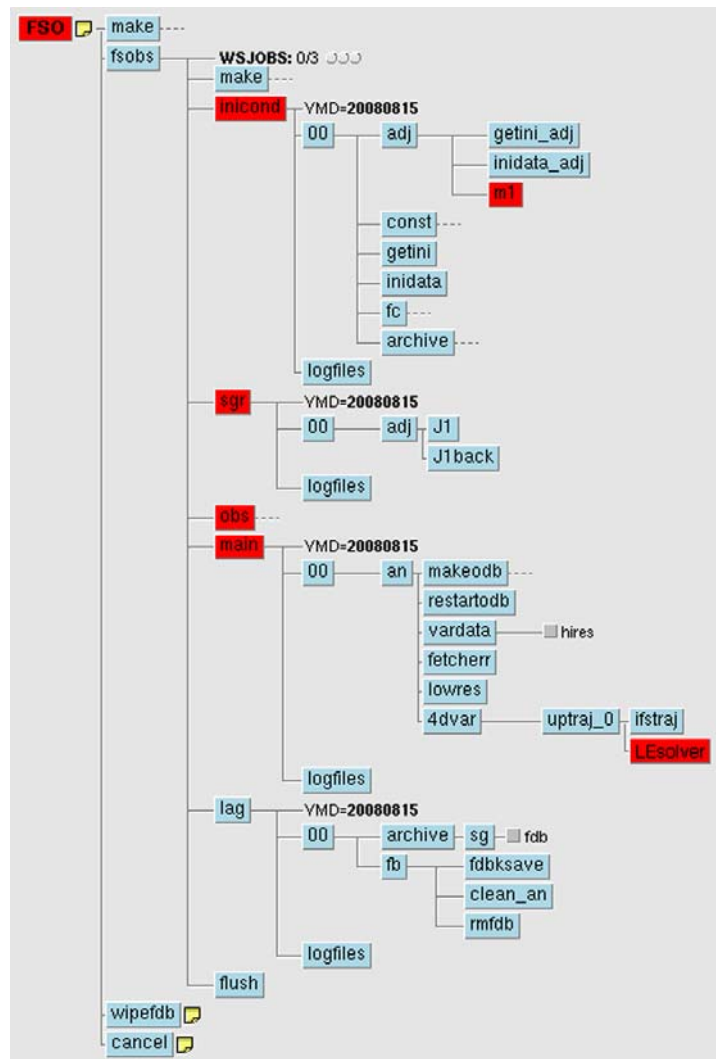


Figure B.1. FSO *sms* configuration

The computational tree comprises few main tasks: *inicond* provides the initial fields for the sensitivity gradient and FSO calculation. The sensitivity gradient calculation (*sgr*) is then performed together with the observation retrieval (*obs*). In the *main* task the linear system is solved (*LEsolver*) after the sensitivity gradients are provided (*sgr*) valid at the beginning of the analysis window (09 or 21 UTC). Task *sgr* and *main* are valid at the same time whilst the forecast error calculation (*inicond-m1*) is valid 24 hour later. Sensitivity gradient and FSO have the same resolution of the analysis from which the forecast error is computed. The operational configuration will then run the forecast field (trajectory) at T799, the linear solver at T255 and 91 model levels. FSO computation is independent of the operational analysis computation being the minimum time lapse of 24 hour (necessary to compute the 24-hour forecast error). The implementation cost on 64MPI and 8 threads is 5644 second wall clock time for the linear equations solver task (to be compared with 3999 second of the minimization task in the analysis experiment) plus 284 second for the

trajectory task. The cost is mainly due to the number of iterations necessary to solve the linear system at the analysis resolution (e.g. last inner loop). The usage of less iteration is under investigation.